21st International Conference on Composite Materials

Xi'an, 20-25th August 2017

UNDERSTANDING STRUCTURAL RECONSTITUTION IN POLYMERIC MATERIALS TO ACHIEVE IN-SITU PROPERTY CONTROL

M. Heili, A. Bielawski, M. Aldridge, K. Sebeck, and J. Kieffer

Department of Materials Science and Engineering
University Of Michigan, Ann Arbor, MI 48109, USA

Keywords: Polymer matrix composites, Relaxation, Interphase, Light scattering, Simulation

ABSTRACT

Using of experimental measurement techniques not commonly used for the investigation of the structure and properties of polymeric materials, namely concurrent inelastic light scattering and tensile testing, in combination with atomic scale simulations, we have gained new insights into structural developments of polymers during cure and in response to mechanical stimuli or spatial constraints. We have identified subtle structural relaxations taking place during cure, which lead to the optimization of molecular packing and ensuing increase in non-bonding interactions. Imposed mechanical strain causes immediate structural reorganization in polymer chains. However, over time, the structure reconstitutes and the original physical properties are recovered. We observe that the reconstitution of entropic aspects of the structure occurs at much higher rates than the reconstitution affecting enthalpic aspects. Spatial confinement, in particular as are established in the interfacial regions of composites, can result in significantly enhanced structural stiffness that is accompanied with a densification of matter. The reason for the improved mechanical properties is the suppression of structurally weak molecular conformations as a result of the confinement.

1 INTRODUCTION

Polymer matrix composites (PMC) are attractive for various structural and functional applications. In view of producing high-strength lightweight material, fiber-reinforced PMC is one of the most promising materials systems. Compared to metals, fiber reinforced PMC can achieve up to tenfold higher specific strength and up to fourfold higher specific stiffness (normalizing with respect to material density) [1]. Beyond lightweight structural materials, PMC applications range from microelectronics devices to medical implants [2–7]. Additional weight savings can be achieved by incorporating auxiliary functionality into the material, such as sensing, actuating, energy harvesting, thermal management, signal processing, etc., which eliminates the need to carry separate devices for these purposes. This opportunity arises from the fact that a composite combines multiple types of materials, with contrasting properties, and without necessarily establishing thermodynamic equilibrium between phases.

Therefore, interfaces, which are an essential feature of composite materials, may not only be disruptive to the transmission of various types of impulses, but they provide the capacity for accommodating functionality that allows one to control and harness these impulses. Indeed, interfaces chiefly determine the properties and performance characteristics of these materials. In many cases, interfaces constitute the origin of materials functionality. Interfaces are not strictly localized to an atomically resolved planar feature, defined by the juxtaposition of chemically distinct species. For one, interfaces possess irregularities, defects, and roughness resulting from processing or materials growth conditions. Secondly, because of the long-range influence of chemical disparity and the inherently non-equilibrium thermodynamic state of materials at interfaces, the structure and properties of specifically the polymer, within a region of significant spatial extent adjacent to the interface, manifestly differ from those of the bulk polymer [8–14].

The existence and spatial extent of this interfacial region, referred to as the interphase, is determined based on the variation in chemical character, e.g., the concentration profile of a telltale species, typically imaged using scanning electron microscopy (SEM) [15–19] or secondary ion mass spectrometry (SIMS) [11, 20], or based on the variation of the polymer's mechanical response, as revealed by nano-indentation using an atomic force microscope [21–24]. Depending on the materials system and technique of investigation, interphase thicknesses between 100 nm and several μm have been reported [25, 26]. Irrespective of size, it is generally believed that the constitution of the interphase chiefly affects the overall mechanical and other properties of the composite [27, 28].

The interphase develops naturally in composites, and although the underlying mechanisms have not yet been systematically established, its formation strongly correlates with the circumstance that materials with dissimilar chemistries are paired. A number of explanations have been proposed. For example, the surface morphology of the embedded phase, such as roughness and pores, promote polymer chain entanglement or limit accessible adsorption area depending on the length of the polymer chains [29–31]. Geometric constraints on the polymer can also create internal stresses in the polymer backbone, resulting in localized residual stress fields at the interface between fiber and polymer [13, 16, 27, 32]. Based on these conjectures, various strategies for altering the surface chemistry of reinforcing fibers have been pursued to improve interfacial properties. Surface treatments, also referred to as sizing, are typically designed to promote covalent bonding between fiber and polymer. Fibers are coated with a strongly adherent thin layer of organic molecules that carry additional reactive functionality to bond with the matrix monomers [11, 33, 34]. Based on their premise, these strategies may be limited to only a few molecular layers adjacent to the interface, but experimental evidence indicates that the structural developments in the entire interphase region may be affected [12, 31, 35]. In fact, surface functionalization and sizing concepts have been expanded to creating interfacial regions with deliberate chemical, structural, and functional gradients [35]. This may involve the coupling between organic and inorganic molecular building blocks to form hybrids in which the intimate juxtaposition of contrasting materials characters affords a tremendous flexibility in controlling thermal and mechanical properties [36–39].

Alternatively, various types of nano-particles are simply added to the thermoset mixture, and one relies on their tendencies to segregate and self-assemble near the interfaces to manipulate interphase properties [40–43]. Significant improvements of the materials properties, such as toughness, tensile strength, elastic moduli, abrasion resistance, etc., have been reported [42, 44]. It is believed that these minuscule particles particularly enhance the interphase region by imparting their own dominant properties [44–48]. For example, embedding carbon nanotubes (CNT) into polymer is done with the expectation that these fillers segregate near the polymer/fiber interface to increase the mechanical strength and thermal conductivity of the interphase, which may have beneficial effects during processing or under operating conditions, or both [49–52].

Evidently, a fundamental understanding of the interfacial structure and phenomena during materials fabrication and application is required. The experimental investigation of interfaces is severely impeded by their minute spatial extend in at least one dimension and by the fact that they are typically

buried, and therefore difficult to access by most characterization techniques. Here we employ a novel combination of inelastic light scattering and tensile testing to characterize the mechanical response of polymeric materials at the molecular scale. In addition, modeling and atomistic simulation provide crucial tools of investigation to complement experiments in revealing the mechanistic underpinnings of the interfacial phenomena by relating the observed phenomena to molecular structure.

2 PROCEDURAL DETAILS

2.1 Sample preparation

In this paper we report on findings for two types of polymeric materials, polyvinylidene fluoride (PVDF), representing chainlike polymers, and epoxy, archetypical for cross-linked polymer networks. PVDF thin films are prepared via solution casting. PVDF powder (Sigma Aldrich, 534,000 MW) is dissolved in N,N-dimethylformamide (DMF) (Sigma Aldrich, 99.8%) at a concentration of 16.7 wt%. The PVDF/DMF mixtures are stirred overnight to obtain homogenous and transparent solution. The solutions are then cast into glass Petri dishes and the DMF is removed at 110°C. The resulting PVDF discs are cut into dogbone shapes using a scalpel. Sample thicknesses are measured using a Fowler electronic dial depth gauge. The thicknesses of all samples are between 0.25 and 0.35 mm.

The epoxy system used for this study is composed of Epon 862 resin (Diglycidyl Ether of Bisphenol F, Hexion Specialty Chemicals) mixed with Epikure 9553 amine hardener (proprietary formulation, Hexion Specialty Chemicals). For the temperature dependent measurements, all samples are mixed using the stoichiometric epoxide to amine ratio recommended by the manufacturer. To prepare each sample for the light scattering measurements, resin and hardener are added to a glass vial such that the desired concentrations of amine and epoxide are available for reaction. The components are mixed by hand for one minute at room temperature. The mixture is then allowed to stand for an additional minute to allow any trapped gas bubbles that formed during the mixing process to escape. Next, the sample is injected into a sample holder composed of a perforated spacer separating two glass coverslips. The sample fills a circular aperture with a 20 mm diameter and 2 mm thickness.

2.2 Materials characterization

For the purpose of this investigation, samples have been characterized using a number of experimental techniques, including thermal analysis to determine glass transition behaviors, x-ray diffraction for the detection of crystalline phases, IR and Raman spectroscopies for the identification of specific molecular groups, phase character, and the degree of cure in the epoxy systems. These techniques are fairly standard methods for materials characterization, and detailed descriptions would surpass the scope of this paper, as they can be readily found in the literature.

Central to this investigation, however, is the unique application of inelastic light scattering for materials characterization, specifically, concurrent Raman (RLS) and Brillouin light scattering (BLS). As the latter technique is perhaps less common, a few words of introduction may be in order. In the BLS experiment, light is used to detect the propagation and attenuation of thermal phonons that exist in any equilibrium condensed phase at finite temperature. No external forcing is required. The spectrum of scattered light contains a peak at a frequency that is Doppler-shifted by ω_S relative to that of the incident light. ω_S is proportional to the velocity of sound, and consequently, the elastic storage modulus of the scattering medium according to $M'(\omega) = \frac{\rho_0 \omega_S^2}{q^2}$ [53]. ρ_0 is the average density of the scattering medium, and q is the wavevector selected by the scattering geometry, $q = 2n/\lambda \sin\theta/2$, where θ is the angle between the incident and scattered light, n is the refractive index of the scattering medium, and λ the wavelength of the light. This technique probes the elastic properties of the structure at the nanoscale, equivalent to subjecting a large number of ~50 nm long dog bone specimens to cyclic tensile tests. Frequency shifts probed by this technique are in the GHz frequency regime, and as a conse-

quence, it yields the adiabatic moduli. This is because, on such a short time scale, heat exchange with the environment is negligible, i.e., $\delta q/T = 0 \Rightarrow dS = 0$. Moreover, the probing light does not impart any significant energy; it does not exert external forcing. Temperature changes are below the detection limit, $c_V dT = 0 \Rightarrow dU = 0$. In other words, the BLS technique is non-invasive, and it measures the adiabatic modulus of a material in thermodynamic equilibrium and at the molecular scale.

2.3 Molecular Simulations

All molecular dynamics (MD) simulations were performed using LAMMPS.[54] Alkane-alkane interactions are controlled with OPLS-AA parameters [55], metal-metal interactions are controlled by the EAM potential [56]. Interactions between the metal substrate and alkane are controlled according to geometric mixing rules using the Lennard-Jones parameters for FCC metal optimized by Heinz et al. [57]. Structures are generated by randomly orienting linear alkane chains at very low density. The fully periodic structure was then gently compressed at elevated temperatures for 60 ps and under constant pressure conditions of about 10 MPa, to accelerate the elimination of the free volume generated the construction of the initial configuration. After this, the simulation box dimensions parallel to the metal substrate are kept constant. The applied pressure is released, and the structure is allowed to relax while zero constant pressure conditions were applied to the direction perpendicular to the substrate only. The resulting structures are then analyzed and subject to various types of non-equilibrium MD runs to determine the desired properties.

3 RESULTS AND DISCUSSION

3.1 Relaxation

Concurrent RLS and BLS was used to monitor the formation of epoxy networks over time, both in terms of the structural connectivity of the network and the evolution of chemical bonding configurations, as well as to measure the visco-elastic properties of the system at the molecular scale. Using this approach we have studied the cure kinetics of epoxy cured with an amine hardener at different temperatures and for a range of epoxy-to-hardener molar ratios [58]. Both factors strongly influence the relationship between the elastic properties of the network and the degree of cure. For a given maximum degree of cure, the resulting epoxy network exhibits the same mechanical properties. The elastic modulus of the epoxy network consist of two contributions: that of network of covalent bonds and that of non-bonded interactions between network segments, which arise when the structure relaxes into an optimally packed configuration. The latter is associated with the so-called relaxational modulus in visco-elastic theory. By probing high-frequency phonons, Brillouin scattering allows one to resolve this relaxational modulus, which is an attribute of a structure in its energy minimum. Static tensile testing, on the other hand, does not resolve the relaxational modulus, as it measures the elastic properties of a structure constrained by the applied stress. Structural changes between relaxed and strained networks are reversible. With increasing rate of cure, the relaxational aspects of network formation become more apparent, because the relaxation process becomes rate limiting in reaching the equilibrium configuration of the network structure. This behavior is summarized in Fig. 1. The unreacted mixture of resin and hardener is a liquid and therefore only exhibits a finite bulk modulus, while the relaxational modulus is essentially zero. As the reaction progresses, cross-links rigidify the structure and the longitudinal modulus gradually deviates from the bulk modulus. If only covalent bonds were to contribute to the structural stiffness, one would observe the static modulus upon completion of the cure, whether it is probed at zero or infinite frequency. However, the structural relaxation that leads to packing optimization and the increase in non-bonding interactions is responsible for the additional elastic energy storage capacity, reflected in the relaxational modulus.

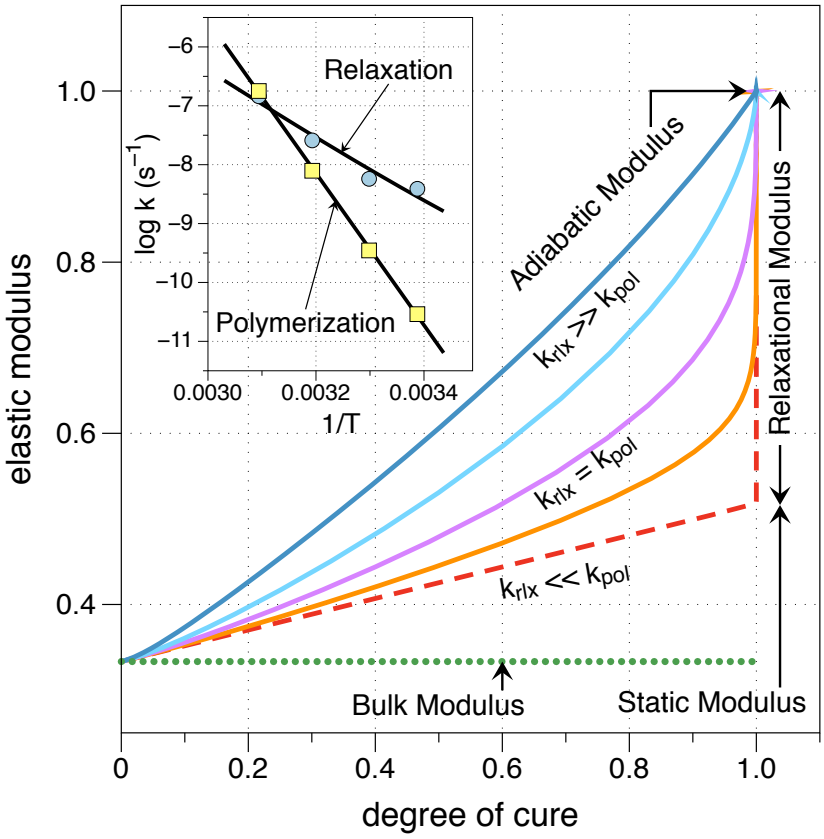

Figure 1: Longitudinal elastic modulus as a function of cure for different cure rates. The curves are derived from the model fit to different data sets, as described in ref. [58]. Inset: Arrhenius plot for the reaction rate coefficient k and the relaxation rate coefficient B. The values of the relaxation rate coefficient have been normalized by the change in modulus due to relaxation at each temperature. This normalization allows us to compare the reaction and relaxation rates on the same scale.

3.2 Reconstitution

To further elucidate the nature of these subtle changes in polymeric materials we displaced two systems, epoxy and PVDF from thermodynamic equilibrium by subjecting them to mechanical strains using a tensile tester, of which the readout provides the stress-strain derived isothermal modulus, while simultaneously measuring the adiabatic properties using BLS. This unique combination of techniques enables concurrent measurement of the adiabatic longitudinal modulus and the isothermal tensile modulus of a sample while it is uniaxially strained. The longitudinal modulus can be measured in the direction parallel or perpendicular to the applied strain as well as any direction in between. Changes in these two moduli are related to stress- and strain-induced microstructural developments. The data in Fig. 2a shows that for PVDF the adiabatic modulus is on average about 4.5 times larger than the isothermal modulus. Upon applying the strain, the both moduli drop immediately. However, while held at the imposed strain, the moduli recover, trending towards their values at zero imposed strain, from which we can conclude that the structure of the material reconstitutes while under this constraint. The relaxation rate describing the time dependence of the isothermal modulus is between one and two orders of magnitude faster than that describing the adiabatic modulus. Note that the isothermal modulus is related to the free energy change of the system due to deformation, while the adiabatic modulus is related to the potential energy change associated with this process. Accordingly, the entropic aspects of the structural deformation recover up to two orders of magnitude more rapidly than the enthalpic aspects.

We observe a similar behavior for the epoxy systems (Fig. 2b). This behavior is consistent with that observed during epoxy cure, in that the applied strain removes the network structure from its ground state configuration, lowering the relaxational component of its elastic modulus by reducing the non-bonding interactions associated with optimal packing. Upon ensuing relaxation, the structure reconstitutes and the system regains the lost elastic energy storage capacity.

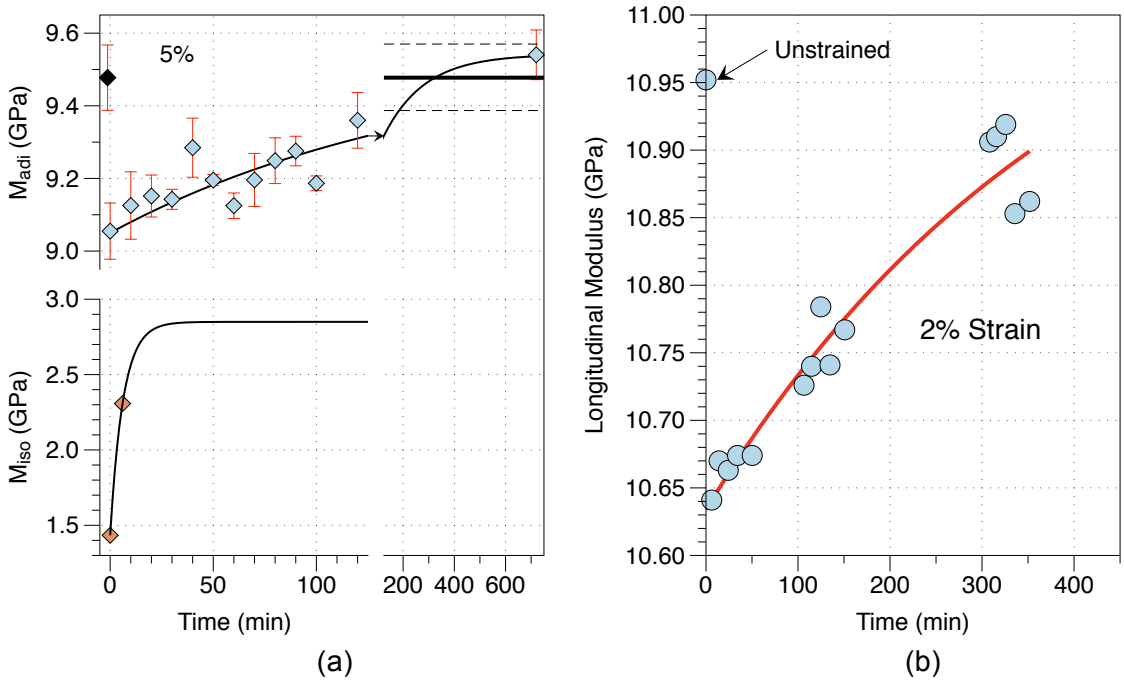

Figure 2 a) Time dependence of the adiabatic (top) and isothermal (bottom) longitudinal elastic moduli of PVDF strained to 5% and then held at that strain for two hours. Data points are fit assuming exponential relaxation with a single rate constant. The last segment shows the relaxation of the modulus for the sample strained to 5% after complete release of this strain; b) Time dependence of the adiabatic modulus and exponential fit of epoxy strained to 2% and held at this train for five hours.

3.3 Structural ordering upon densification

Experimental results are complemented with information provided by molecular dynamics simulations. This is particularly useful for the investigation of interfacial regions in polymer matrix composites, which are difficult to access experimentally. Using simulations, we have investigated the structural developments in alkane polymer adjacent to an interface with a metal substrate, by systematically varying the alkane chain length, the substrate lattice parameter, and, in a parametric fashion, the substrate-alkane interaction strength [59]. The structure of the alkane film near an interface has been examined according to a variety of metrics. In all cases we observed a strongly pronounced layering of the alkanes near the interface, which is associated with an optimized packing of the chains within the layer planes, leading to a density increase of up to four times the bulk alkane density (Fig. 3a). The peak density exhibits a logarithmic dependence on the interaction strength between metal and alkane, reflecting the saturation in the ability for alkane chains to pack onto the substrate surface, while the inter-chain spacing follows the inverse trend. The lattice parameter of an fcc metal substrate has the potential to accentuate both dependencies, but the range of experimentally observed interaction strengths is comparably limited. In all cases, the magnitude of the structural variation is increased for shorter chain lengths. Longer chains show more entanglement between layers, implying a stronger effect on macroscopic properties for smaller molecules. The layering, densification, and lateral confinement at interfaces also enhance the mechanical stiffness of the alkane phase. Most surprisingly, this increase in elastic modulus is characteristic of the interfacial structure even beyond the region affected by the obvious layering and densification. The most likely reason for this effect is a confine-

ment-induced suppression of *cis* conformations in the polymer chains, which eliminates inherently unstable segment orientations that directly detract from the structural stiffness, and which affect the polymer phase to an extent that is neither visually apparent, nor is it evident when applying lower-order measures of structural characterization measures. However, two-dimensional pair correlation functions with slices parallel to the interface and similarly parsed backbone dihedral angle analyses provide evidence for such structural features. Accordingly, insertion of small concentrations of nano-particles, whose surfaces can serve as templates for the polymer assembly, can dominate the structural evolution within the interphase and, according to our findings, have dramatic effects on the mechanical properties – a phenomenon that is already well known from experiments.

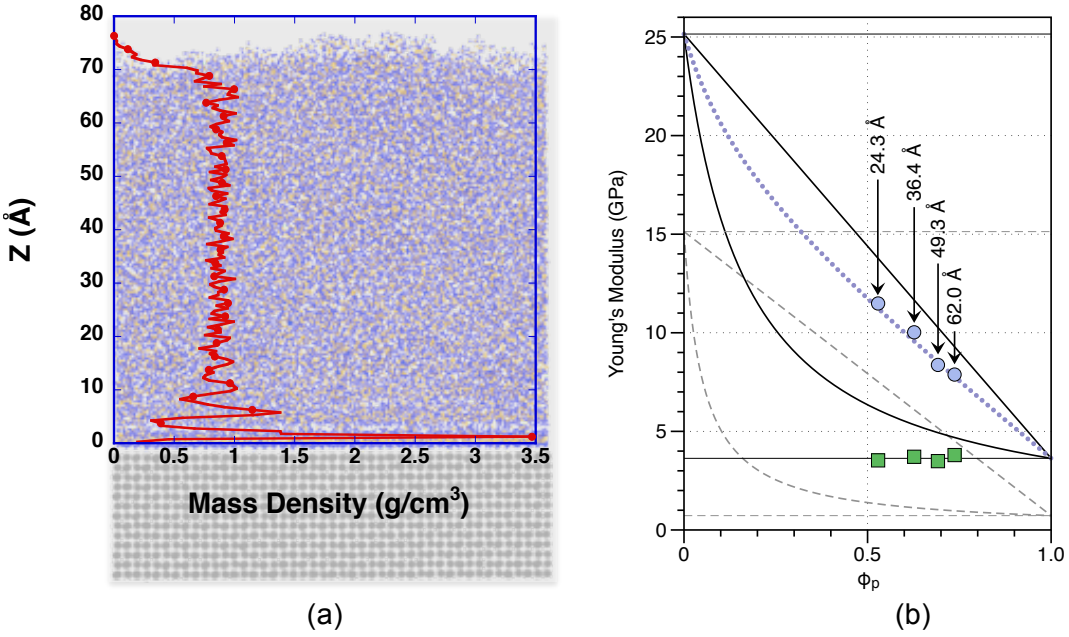

Figure. 3 a) Density profile in an alkane (n=20) film as a function of the distance from the interface with a Cu substrate; b) Composite elastic moduli for different layer thicknesses from simulation as a function of the alkane volume fraction (circles); the modulus of the alkane segment, considering stresses and strains in that phase only, are shown as squares. The elastic modulus for the Cu segment in our simulations is 25.15 GPa. Two rules-of-mixture constructs are provided for reference: the dashed lines are based on the elastic moduli of the pure phases computed for their respective bulk configurations and the solid lines are based on the moduli computed for the respective segments in the laminates.

4 CONCLUSIONS

Polymer structures displaced from equilibrium, either as a result of undergoing polymerization and cross-linking reactions that result in network structure where its constituents initially end up slightly removed from their ground state configuration, or when subjecting fully cured networks to elastic strains, tend to reconstitute so as to optimize molecular packing and maximize non-boning interactions (minimize their potential energy), which in turn results in an enhanced capacity for elastic energy storage. Molecular simulations show that the optimization of molecular packing, in this case achieve through the adhesive forces exerted by a nearby substrate, tend to significantly enhance the elastic moduli of these structure, even beyond the range that is measurably densified. This is due to the fact that packing optimization causes the elimination of mechanically unstable molecular conformations.

5 ACKNOWLEDGEMENTS

This work was supported by the National Science Foundation, grant no. CBET 1402845, and the Air Force Office for Scientific Research, grant no. FA9550-14-1-0010.

6 REFERENCES

[1] Brinson, L. C., K. L. Reifsnider, P. A. Bartolotta, M. B. Buczek, J. W. Davis, N. J. Johnston, A. M. Sastry, and S. S. Sternstein. 2005. *Going to Extremes: Meeting the Emerging Demand for Durable Polymer Matrix Composites*. National Academic Press, Washington, D.C.

[2] Bagheri, R., B. T. Marouf, and R. A. Pearson Rubber-Toughened Epoxies: A Critical Review *Polymer Reviews* 49, 2009 201-225.

[3] Bartus, S. D. A review: Impact damage of composite materials *Journal of Advanced Materials* 39, 2007 3-21.

[4] Qiao, P. Z., M. J. Yang, and F. Bobaru Impact mechanics and high-energy absorbing materials: Review *Journal of Aerospace Engineering* 21, 2008 235-248.

[5] Sun, L. Y., R. F. Gibson, F. Gordaninejad, and J. Suhr Energy absorption capability of nanocomposites: A review *Composites Science and Technology* 69, 2009 2392-2409.

[6] Wong, C. P., and M. M. Wong Recent advances in plastic packaging of flip-chip and multichip modules (MCM) of microelectronics *IEEE Transactions on Components and Packaging Technologies* 22, 1999 21-25.

[7] Wu, D. Y., S. Meure, and D. Solomon Self-healing polymeric materials: A review of recent developments *Progress in Polymer Science* 33, 2008 479-522.

[8] Brodowsky, H. M., W. Jenschke, and E. Mader Characterization of Interphase Properties by Frequency-Dependent Cyclic Loading of Single Fibre Model Composites *J Adhes Sci Technol* 24, 2010 237-253.

[9] Gohil, P. P., and A. A. Shaikh Analytical Investigation and Comparative Assessment of Interphase Influence on Elastic Behavior of Fiber Reinforced Composites *J Reinf Plast Comp* 29, 2010 685-699.

[10] Jancar, J. Review of the role of the interphase in the control of composite performance on micro- and nano-length scales *J. Mater. Sci.* 43, 2008 6747-6757.

[11] Jones, F. R. A Review of Interphase Formation and Design in Fibre-Reinforced Composites *J Adhes Sci Technol* 24, 2010 171-202.

[12] Liu, L., Y. J. Song, H. J. Fu, Z. X. Jiang, X. Z. Zhang, L. N. Wu, and Y. D. Huang The effect of interphase modification on carbon fiber/polyarylacetylene resin composites *Appl. Surf. Sci.* 254, 2008 5342-5347.

[13] Maligno, A. R., N. A. Warrior, and A. C. Long Effects of interphase material properties in unidirectional fibre reinforced composites *Compos Sci Technol* 70, 2010 36-44.

[14] Ostad-Movahed, S., A. Ansarifar, and M. Song Effects of Different Interphases on the Mechanical Properties of Cured Silanized Silica-Filled Styrene-Butadiene/Polybutadiene Rubber Blends for Use in Passenger Car Tire Treads *J. Appl. Polym. Sci.* 113, 2009 1868-1878.

[15] Kieffer, A., and A. Hartwig Interphase reaction of isocyanates with epoxy resins containing functional groups of different reactivity *Macromolecular Materials and Engineering* 286, 2001 254-259.

[16] Bouchet, J., A. A. Roche, and E. Jacquelin How do residual stresses and interphase mechanical properties affect practical adhesion of epoxy diamine/metallic substrate systems? *Journal of Adhesion Science and Technology* 16, 2002 1603-1623.

[17] Muller, U., R. Bactavatchalou, J. Baller, M. Philipp, R. Sanctuary, B. Zielinski, P. Alnot, W. Possart, and J. K. Kruger Acoustic profilometry of interphases in epoxy due to segregation and diffusion using Brillouin microscopy *New Journal of Physics* 10, 2008 023031.

[18] Meiser, A., C. Kubel, H. Schafer, and W. Possart Electron microscopic studies on the diffusion of metal ions in epoxy-metal interphases *Int J Adhes Adhes* 30, 2010 170-177.

[19] Sperandio, C., C. Arnoult, A. Laachachi, M. Di, J, and D. Ruch Characterization of the interphase in an aluminium/epoxy joint by using controlled pressure scanning electron microscopy

coupled with an energy dispersive X-ray spectrometer *Micron* 41, 2010 105-111.

[20] Swait, T. J., T. Whittle, C. Soutis, and F. R. Jones Identification of interfacial and interphasal failure in composites of plasma polymer coated fibres *Composites Part A-Applied Science and Manufacturing* 41, 2010 1047-1055.

[21] Yedla, S. B., M. Kalukanimuttam, R. M. Winter, and S. K. Khanna Effect of shape of the tip in determining interphase properties in fiber reinforced plastic composites using nanoindentation *J Eng Mater-T ASME* 130, 2008 ARTN 041010.

[22] Ramos, J. A., M. Blanco, I. Zalakain, and I. Mondragon Nanoindentation study of interphases in epoxy/amine thermosetting systems modified with thermoplastics *J Colloid Interf Sci* 336, 2009 431-437.

[23] Monclus, M. A., T. J. Young, and M. Di, D AFM indentation method used for elastic modulus characterization of interfaces and thin layers *J. Mater. Sci.* 45, 2010 3190-3197.

[24] Zhao, W., and C. S. Korach Measurement of Epoxy Stiffness By Atomic Force Acoustic Microscopy *Proceedings of the ASME International Mechanical Engineering Congress and Exposition* 12, 2010 85-87.

[25] Buryan, O. K., and V. U. Novikov Modeling of the interphase of polymer-matrix composites: Determination of its structure and mechanical properties *Mechanics of Composite Materials* 38, 2002 187-198.

[26] Kim, J. K., and A. Hodzic Nanoscale characterisation of thickness and properties of interphase in polymer matrix composites *Journal of Adhesion* 79, 2003 383-414.

[27] Bouchet, J., A. A. Roche, and E. Jacquelin Determination of residual stresses in coated metallic substrates *Journal of Adhesion Science and Technology* 15, 2001 321-343.

[28] Kim, W. S., and J. J. Lee Adhesion strength and fatigue life improvement of co-cured composite/metal lap joints by silane-based interphase formation *Journal of Adhesion Science and Technology* 21, 2007 125-140.

[29] Gao, X., R. E. Jensen, W. Li, J. Deitzel, S. H. McKnight, and J. W. Gillespie Effect of fiber surface texture created from silane blends on the strength and energy absorption of the glass fiber/epoxy interphase *Journal of Composite Materials* 42, 2008 513-534.

[30] He, J. M., and Y. D. Huang AFM characterization of interphase properties of silver-coated carbon fibre reinforced epoxy composites *Polym Polym Compos* 14, 2006 123-133.

[31] Zhang, J., Q. P. Guo, M. Huson, I. Slota, and B. Fox Interphase study of thermoplastic modified epoxy matrix composites: Phase behaviour around a single fibre influenced by heating rate and surface treatment *Composites Part A-Appled Science and Manufacturing* 41, 2010 787-794.

[32] Jiang, Y. P., W. L. Guo, and H. Yang Numerical studies on the effective shear modulus of particle reinforced composites with an inhomogeneous inter-phase *Comp. Mater. Sci.* 43, 2008 724-731.

[33] Mader, E., and S. L. Gao Prospect of nanoscale interphase evaluation to predict composite properties *J Adhes Sci Technol* 15, 2001 1015-1037.

[34] Yang, Y., C. X. Lu, X. L. Su, and X. K. Wang Effects of emulsion sizing with nano-SiO2 on interfacial properties of carbon fibers/epoxy composites *J. Mater. Sci.* 42, 2007 6347-6352.

[35] Leonard, G. C., D. Hosseinpour, and J. C. Berg Modulus-Graded Interphase Modifiers in E-Glass Fiber/Thermoplastic Composites *J Adhes Sci Technol* 23, 2009 2031-2046.

[36] Jabbour, J., S. Calas, S. Gatti, R. K. Kribich, M. Myara, G. Pille, P. Etienne, and Y. Moreau Characterization by IR spectroscopy of an hybrid sol-gel material used for photonic devices fabrication *J. Non-Cryst. Solids* 354, 2008 651-658.

[37] Nagendiran, S., M. Alagar, and I. Hamerton Octasilsesquioxane-reinforced DGEBA and TGDDM epoxy nanocomposites: Characterization of thermal, dielectric and morphological properties *Acta Mater.* 58, 2010 3345-3356.

[38] Nazir, T., A. Afzal, H. M. Siddiqi, and Z. Ahmad Thermally and mechanically superior hybrid epoxy-silica polymer films via sol-gel method *Progress in Organic.* 2010

[39] Versace, D. L., A. Chemtob, C. Croutxe-Barghorn, and S. Rigolet Synthesis of Organosilica Films Through Consecutive Sol/Gel Process and Cationic Photopolymerization *Macromol Mater Eng* 295, 2010 355-365.

[40] Auad, M. L., M. A. Mosiewicki, C. Uzunpinar, and R. J. J. Williams Functionalization of Car-

bon Nanotubes and Carbon Nanofibers Used in Epoxy/Amine Matrices That Avoid Partitioning of the Monomers at the Fiber Interface *Polym. Eng. Sci.* 50, 2010 183-190.

[41] Brownlow, S. R., A. P. Moravsky, N. G. Kalugin, and B. S. Majumdar Probing deformation of double-walled carbon nanotube (DWNT)/epoxy composites using FTIR and Raman techniques *Compos Sci Technol* 70, 2010 1460-1468.

[42] Mao, D. S., Z. Yaniv, R. Fink, and L. Johnson Carbon Nanotube-reinforced Epoxy Nanocomposites for Mechanical Property Improvement *Nanotech Conference & Expo 2009* 3, 2009 461-464.

[43] Shen, S. Z., S. Bateman, C. Huynh, M. Dell'Olio, S. Hawkins, W. D. Yang, Q. Y. Yang, and K. F. Cai Impact of Carbon Nanotube Aspect Ratio and Dispersion on Epoxy Nanocomposite Performance *Adv Mat Res* 66, 2009 198-201.

[44] Wang, X., H. M. Liu, P. F. Fang, L. M. Liao, C. X. Pan, and K. M. Liew Interface Enhancement of Glass Fiber/Vinyl Ester Composites with Carbon Nanotubes Synthesized from Ethanol Flames *J. Nanosci. Nanotech.* 10, 2010 948-955.

[45] Ciprari, D., K. Jacob, and R. Tannenbaum Characterization of polymer nanocomposite interphase and its impact on mechanical properties *Macromolecules* 39, 2006 6565-6573.

[46] Gao, S. L., and E. Mader Characterisation of interphase nanoscale property variations in glass fibre reinforced polypropylene and epoxy resin composites *Composites Part A-Applied Science and Manufacturing* 33, 2002 559-576.

[47] Kim, J. K., M. L. Sham, and J. S. Wu Nanoscale characterisation of interphase in silane treated glass fibre composites *Composites Part A-Applied Science and Manufacturing* 32, 2001 607-618.

[48] Williams, J. G., F. P. Li, and I. Miskioglu Characterization of the interphase in epoxy/aluminum bonds using atomic force microscopy and a nano-indenter *Journal of Adhesion Science and Technology* 19, 2005 257-277.

[49] Davis, D. C., J. W. Wilkerson, J. A. Zhu, and D. O. O. Ayewah Improvements in mechanical properties of a carbon fiber epoxy composite using nanotube science and technology *Compos Struct* 92, 2010 2653-2662.

[50] Montazeri, A., and R. Naghdabadi Investigation of the Interphase Effects on the Mechanical Behavior of Carbon Nanotube Polymer Composites by Multiscale Modeling *J. Appl. Polym. Sci.* 117, 2010 361-367.

[51] Needleman, A., T. L. Borders, L. C. Brinson, V. M. Flores, and L. S. Schadler Effect of an interphase region on debonding of a CNT reinforced polymer composite *Composites Science and Technology* 70, 2010 2207-2215.

[52] Qian, H., A. Bismarck, E. S. Greenhalgh, and M. S. P. Shaffer Carbon nanotube grafted carbon fibres: A study of wetting and fibre fragmentation *Composites Part A-Aapplied Science and Manufacturing* 41, 2010 1107-1114.

[53] Kieffer, J. 2015. Brillouin Light Scattering. In *Modern Glass Characterization*, M. Affatigato, ed. Wiley & Sons, Hoboken, NJ, p. 107-155.

[54] Plimpton, S. Fast Parallel Algorithms for Short-Range Molecular Dynamics *J Comp Phys* 117, 1995 1-19.

[55] Jorgensen, W. L., and J. Tirado-Rives The OPLS potential functions for proteins. Energy minimizations for crystals of cyclic peptides and crambin *J. Am. Chem. Soc.* 110, 1988 1657-1666.

[56] Foiles, S. M., M. I. Baskes, and M. S. Daw Embedded-atom-method functions for the fcc metals Cu, Ag, Au, Ni, Pd, Pt and their alloys *Phys. Rev. B* 33, 1986 7983.

[57] Heinz, H., R. A. Vaia, B. L. Farmer, and R. R. Naik Accurate Simulation of Surfaces and Interfaces of Face-Centered Cubic Metals Using 12− 6 and 9− 6 Lennard-Jones Potentials *The Journal of Physical Chemistry C* 112, 2008 17281-17290.

[58] Aldridge, M., A. S. Wineman, A. M. Waas, and J. Kieffer In Situ Analysis of the Relationship between Cure Kinetics and the Mechanical Modulus of an Epoxy Resin *Macromolecules* 47, 2014 8368-8376.

[59] Sebeck, C., C. Shao, and J. Kieffer Alkane-Metal Interfacial Structure and Elastic Properties by Molecular Dynamics Simulation *ACS Applied Materials and Interfaces* 8, 2016 16885-16896.